GEOFIZIKA VOL. 39 2022

DOI: https://doi.org/10.15233/gfz.2022.39.2
Original scientific paper

Biexponential decrease of PAR in coastal waters (Northern Adriatic)

Borut Umer [1,2] *and Vlado Malačič* [1]

[1] National Institute of Biology, Marine Biology Station, Piran, Slovenia

[2] Jožef Stefan international Postgraduate School, Ljubljana, Slovenia

Received 12 February 2021, in final form 7 June 2021

The attenuation coefficients of photosynthetically active radiation (PAR) were extracted from the vertical profiles of PAR in coastal waters (the Gulf of Trieste, Northern Adriatic). The vertical profiles were collected roughly twice per month from July 2011 to December 2015, and the PAR values just above the sea surface were compared with the PAR data measured on a buoy.

This research supports the nonlinear fit with the biexponential expression for the dependence of PAR with depth, yielding a much better match with the data than the fit with a mono-exponential expression. However, another reasoning for biexponential attenuation is because it functions as a solution for a homogeneous differential equation of a second order. The method for estimating the water type is offered with an analysis of the attenuation coefficients of PAR. It was found that for a particular location (the Gulf of Trieste), the attenuation coefficient in a mono-exponential decrease of PAR is 0.19–0.21 $m^{-1,}$ while for a biexponential decrease of PAR, the coefficient of the long-range attenuation is 0.12–0.14 m^{-1} and that of short-range attenuation is 0.8–0.9 m^{-1}. This leads to the conclusion that most water columns match coastal water type 1, while the surface layer is represented by coastal water types 7 or 9. From the estimate of the water types, the coefficients of downward irradiation were inferred as 0.19 m–1 ± 0.01 m^{-1} (long-range attenuation) and 3.0 m^{-1} ± 0.7 m^{-1} (short-range attenuation). These coefficients can deter-mine the heat source inside the water column.

Keywords: PAR, attenuation coefficient, irradiation, Secchi disk depth, fitting methods

1. Introduction

In marine ecology and marine environmental monitoring, one of the most common methods for measuring the "light conditions" or transparency of natural waters in the water's surface layers is the simple Secchi disk depth, which dates

back to 1864 (Secchi, 1864). With this method, the depth at which a white plate 0.3 m in diameter vanishes from sight is measured. Another widely applied method is measuring the photosynthetically active radiation (PAR) (I), which determines the rate at which photons hit a sensor with energies corresponding to wavelengths of light between 400 and 700 nm (Kirk, 1994). Talley (2011) attempts to merge the Secchi disk depth with the vertical profile of downward irradiance. The link between the Secchi disk depth and the visibility of submerged objects has been pointed out by Duntley and Preisendorfer (1952), in which the visibility attenuates exponentially with the coefficients of collimated and diffuse light. For (downward) irradiance, in Talley (2011), the exponential decrease is presumed to be the coefficient of diffuse light. The exponential attenuation of downward energy (irradiance) in a visible spectrum has otherwise been frequently used (Jerlov, 1976; Kirk, 1994; Lee et al., 2005; Talley et al., 2011). A recent review by Lee et al. (2018) explores the relationship between the diffusion attenuation coefficient of the PAR and Secchi disk depth, including an exhaustive study that relates the quantities derived by satellite measurements (absorption and backscattering coefficients), which depend on the wavelength of the penetrating (and backscattered) light and that represent the inherent optical properties (IOPs) of the water column. In the current paper, a novel explanation of the attenuation coefficients in the nonlinear analytical expressions of I is offered. Also, a new concept for estimating the coefficients of the total downward irradiance of light is presented by determining the water type (Jerlov, 1976) with I. The "Jerlov" classification is somewhat outdated, as pointed out by Lee et al. (2005); however, it is still in use in numerical models of ocean circulation (Hedström, 2009; Mellor, 2004) when it comes to measuring the heat and stratification of a water column with solar radiation. Recent numerical models still combine the biexponential expression for the downward irradiance with this classification of water types as one of the ways to describe the downward irradiance in seawaters (see Madec et al. (2019), the subsection 4.4.2 Solar radiation penetration), where the attenuation coefficients must be known.

Numerous vertical profiles of the PAR in the inner part of the Gulf of Trieste (Northern Adriatic) can be found in Stravisi (1999). An exponential decline with depth is also assumed for the PAR part of the visible spectrum of light. The Secchi disk depth Z_S has been connected to the PAR attenuation coefficient k as $k = P/Z_S$, where $P = 1.4 \pm 0.2$. Values of the proportionality factor are reviewed in Tab. 1 of Lee et al. (2018). Working within this context, the current paper extends the work of Stravisi by studying the biexponential damping of PAR, and the value of the coefficient P is evaluated.

It was established in the 1970s (Paulson and Simpson, 1977) that the biexponential decrease of downward irradiance is a much better representation of the attenuation of light with depth. Because a decrease in downward irradiance with depth is related to heating the water column, the biexponential representation can also be applied in numerical models of circulation (Meier, 2001; Mellor,

2004). A review of the PAR parametrization in Byun et al. (2014) also suggests that a biexponential expression is a better match with the data. However, the expression suggested in Byun et al. (2014) is redundant when it comes to the coefficients, and a slightly simplified version fits the data better.

We also explore the classification of water types according to Jerlov (1976), which is defined based on the vertical profiles of downward irradiance, as well as on the vertical profiles of the PAR. By fitting the vertical profiles of the PAR for each water type with the biexponential function, we show the typical values of two attenuation coefficients that enable the classification of the water type of the Gulf of Trieste in the Northern Adriatic. By knowing the water type, we can then easily retrieve the coefficients for the decrease in downward irradiance, which turns into heat. The flowchart of the procedure is presented in Fig. 1.

This is an important added value of the concept because measurements of downward irradiance from which the attenuation coefficients are otherwise revealed are much more demanding and expensive. Therefore, they are rarely performed when it comes to simpler PAR measurements. These coefficient values are applied in numerical modeling of the circulation of coastal waters. Finally, we present the relationship between the Secchi disk depth and the attenuation coefficient in a single exponential.

In the methods section, the expressions for exponential attenuation and biexponential attenuation are presented, along with the reasoning for both of them in a differential form. Preprocessing of the PAR measurements is also

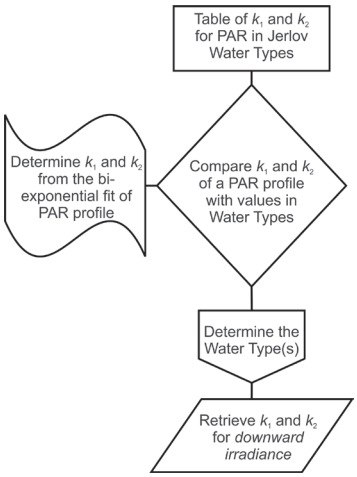

Figure 1. Flowchart of the steps leading to the determination of the downward irradiance. k_1 and k_2 are the attenuation coefficients of the long- and short-range parts of the attenuation of the PAR and the downward irradiance, respectively. The table of water types and corresponding attenuation coefficients of the PAR can be found in Tab. 6 (first panel), while the attenuation coefficients of the downward irradiance can be found in Tab. 7 (bottom panel).

described. In the results section, the key findings of fitting the PAR data are presented, while in the summary and discussion, the results are discussed with a reasonable conjecture about the water type of the Gulf of Trieste.

2. Methods

2.1. PAR measurements

PAR measurements were conducted in the air above the sea surface, as well as in the water column. PAR measurements in the air were conducted with two PAR sensors, both from the manufacturer Li-COR (Anon., 2006a). The first (Li-COR LI 190 SL 50) was mounted on the coastal buoy "Vida" (see Fig. 2, PAR sensor marked with a red arrow) located in the northernmost part of the Adriatic Sea, the Gulf of Trieste, while the second (Li-COR LI 192 SA) was installed on a Sea & Sun Technology microstructure probe MSS90 (Anon., 2006b, 2007), which is visible in Fig. 3, outlined with a red circle.

This one is more frequently used for measurements in water (Anon., 2006a). The MSS90 probe was cast in free-falling mode for vertical profiling of the water column around the buoy Vida at a distance of about 100 m. The PAR sensor on

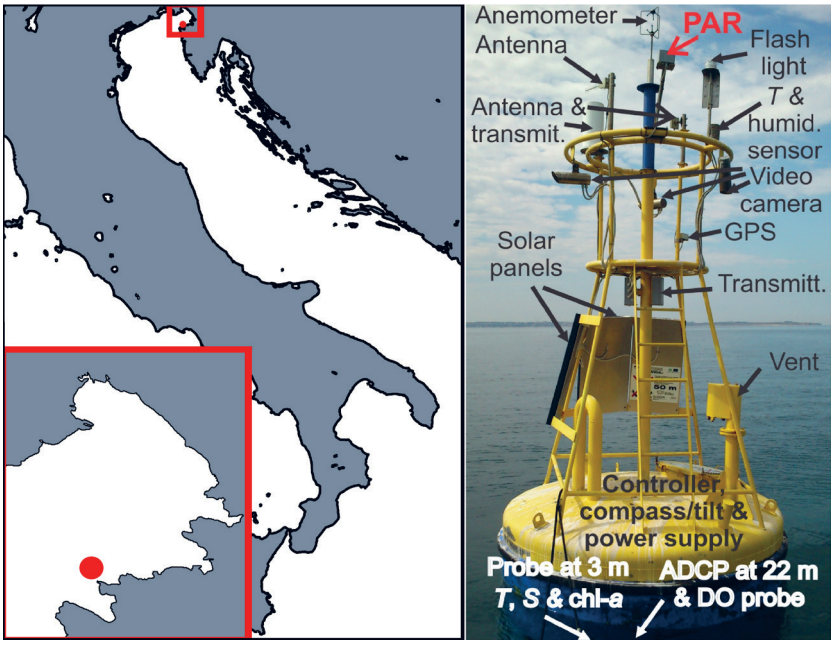

Figure 2. *Left*: Area of interest. The red dot represents the location of the buoy Vida (13° 33.042' E, 45° 32.925' N) in the Gulf of Trieste (Northern Adriatic). *Right*: Buoy Vida with PAR sensor at a height of 4.5 m.

Figure 3. PAR sensor (*left*; circled with a red line) on top of a microstructure probe (*right*).

buoy Vida was mounted at a height of 4.5 m. Its data streamed with a frequency of 4.26 Hz to the receiving station on land 3.7 km away. Taking into account winds and waves, the motion of the buoy Vida is described in Malačič (2019). Tilting of the PAR sensor on the buoy was effectively removed by 15 min averaging the instantaneous (4.26 Hz) PAR data.

Both sensors were cosine corrected (Anon., 2005, 2006a). Because LI-192 can be applied to measurements of PAR in water and air, the manufacturer provides two sets of calibration (sensitivity) constants: one for air and another for water. It follows from the calibration that sensitivity in air is larger than in water by a factor of 1.32, which we considered in the postprocessing of the PAR data that was taken from the free-falling probe.

During the free fall of the probe, which was released from the research boat, the probe recorded data from each sensor at a frequency of 1024 Hz (Anon., 2006b). Before the vertical cast, the probe needed to stabilize the response of the underwater sensors (*e.g.*, temperature, conductivity, dissolved oxygen) in water for several minutes when the PAR sensor on top of the hanging probe was still in the air. Then, the 1.53 m long MSS 90 probe (GmbH, 2021) hanged on a rope before being cast from a side bank of a vessel in such a way that only about a fifth of the probe was lowered into the water—specifically, its marine sensors. After a few minutes of compensation, the recording of the data started when the PAR sensor was still in the air and the probe was manually lowered for about 0.5–1.0 m. When the probe was released into a free fall, the PAR data for which the pressure sensor at the bottom of the probe recorded pressures < 1.2 dbar,

which became the PAR data in the air, because the vertical distance between the PAR sensor and the pressure sensor was 1.2 m. This has been accounted for in the data pairs (depth, PAR). During the free fall casts, the tilt was relatively low (less than 3°), and the falling speed of the probe (around 0.7 m/s) was determined by the weights, which were placed on a housing just above the sensors and on the floats just below the top of the housing.

The PAR sensor on the buoy Vida has been in operation since 2011; therefore, for comparison with the PAR on the probe on board of a vessel, 59 vertical casts performed between 14 July 2011 and 16 December 2015 were carried out. The minimum time the PAR sensor spent in the air while the data were recorded was 2.2 s, while the maximum time was 15.3 s, with a mean value of 7.7 s (median 7.4 s) and a standard deviation of 3.4 s. This means that the average time for the PAR measured above sea level in the air was > 2 s, which is a typical (largest) period of waves during "nice" weather conditions (sea state "3" at most), which is a prerequisite for a cruise campaign.

Each freefall cast of the MSS probe was complemented with a visual estimation of the depth of the white Secchi disk plate, which was lowered on the side of a vessel in the shade. The error of the Secchi depth, which reached 15 m at most, was estimated to be 0.3 m.

The PAR vertical profiles were taken every fortnight near the buoy Vida for the period 25 February 2010 to 16 December 2015. The "raw" PAR values for each PAR profile, which were collected with vertical resolution of the order 10^{-3}–10^{-2} m, were averaged over depth intervals of 0.1 m, here starting with the depth $z_0 = -0.1$ m. In this way, the statistics of the PAR profiles could be obtained, and high-frequency oscillations of PAR within depth intervals of 0.1 m were removed because they did not contribute to PAR behavior over a 20 m depth range.

The number of "reliable" PAR profiles in which the PAR monotonously decreased with depth was much smaller than expected. The vertical PAR profiles may have experienced a lot of "wiggling" values with increasing depth, or they may not have been decreasing monotonously with depth. Dubious profiles were obtained mostly by casting the probe on the shaded side of the research vessel. The probe may have "fallen out" of the shadow zone at a certain depth; therefore, their PAR would increase with depth.

Profiles for which PAR did not decrease with depth in the years 2010 and 2015 are marked as "dubious," as seen in Tab. 1.

Table 1. Dubious and reliable PAR profiles between 25 February 2010 and 16 December 2015.

	Season				
Type	Spring	Summer	Autumn	Winter	All
Reliable	17	21	26	17	81
Dubious	16	11	6	7	40

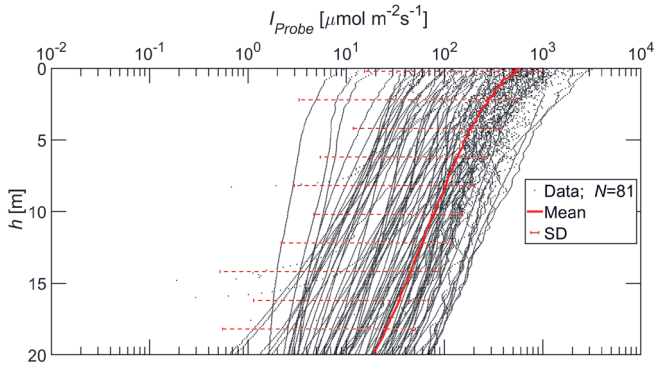

Figure 4. PAR profiles between 25 February 2010 and 16 December 2015 that were applied in the analysis.

The remaining 81 PAR profiles presented here were taken in the morning between 7:13 h and 11:29 h CET (Central European time, which equals the local solar time), with a mean time and standard deviation of 9:02 h ± 0:53 h and a median of 8:49 h. This morning time has already yielded an impression about the relatively modest solar elevation above the horizon. Still, calculations of the solar elevation for 81 casts (https://www.esrl.noaa.gov/gmd/grad/solcalc/calcdetails.html) reveal that the mean solar elevation and its standard deviation are 26.5° ± 10.9°, with a median value of 27.1°. Less than 4.9% – or four of all considered casts – were taken with an elevation of ≤ 12°. Therefore, the solar elevation during casts was well above this lower limit (the refraction in the atmosphere contributes about 1°). The data regarding cloud conditions are missing. However, they would not reveal whether there was also a direct solar impact on the sea surface or only the diffuse (PAR) light. The presence of the latter and lack of the former are simply reflected in the low PAR values of a few 10 µmol m^{-2} s^{-1} in the air above the sea surface. Therefore, all considered PAR profiles captured a variety of direct and diffuse light.

Among the 81 PAR profiles, at each 0.1 m depth, the mean PAR value and the standard deviation (SD) have been calculated, leading to the mean vertical PAR profile on Fig. 4 (red full line). The SDs at each depth are presented with horizontal red dashed lines. The bottom depth (21 m ± 1 m) varied mainly because of tides; therefore, the uniform maximum depth of the PAR profiles was chosen as 20 m.

2.2. Analytical expressions of PAR attenuation

We should highlight the link between the analytical expression of the downward attenuation of light in the sea and its differential form. The simple exponential decrease with the depth (= $-z$) of the PAR $I = I_0 e^{kz}$ ($z < 0$), in which I_0 is the PAR just below the sea surface, and k is the depth independent coefficient of

attenuation, follows as a solution of the differential equation (Beer's law) of the first order (Jerlov, 1968, 1976; Kirk, 1994; Talley, 2011; Talley et al., 2011)

$$\frac{dI}{dz} = kI \,. \tag{1}$$

In our study, we have calculated the single-exponential decrease in the PAR in two different ways: first, by using the linear semilog expression and, second, by using the nonlinear fitting of the exponential function with the initial value for k provided by the semilog fitting.

However, the biexponential decrease in I:

$$I(z) = I_1 e^{k_1 z} + I_2 e^{k_2 z} \,, \tag{2}$$

has not yet been expressed in equivalent differential form. (2) was proposed by Paulson and Simpson (1977) for downward irradiance, where the first parameter characterizes the rapid attenuation in the upper 5 m because of the absorption of the red end of the spectrum and where the second parameter represents the attenuation of blue-green light below 10 m. Similarly, Byun et al. (2014) applied expression (2) for the downward penetration of the PAR. It is the solution for

$$A\frac{d^2 I}{dz^2} + B\frac{dI}{dz} + CI = 0 \,, \tag{3}$$

in which we assume $A > 0$. Its derivation is left for Appendix A. Here, we only point out that it follows from expression A3 that the rate of decrease of I with z, that is, dI/dz is a function $Y(z)$, where its rate dY/dz is a linear superposition of the function Y itself and I. The coefficient of proportionality next to Y is the sum of the attenuation coefficients $k_1 + k_2$, while the coefficient next to I is their product $k_1 k_2$.

However, the physical concept behind (3) is not offered in the references that describe the exponential decrease of light (1). It can be shown that (3) is based on a twofold application of Beer's law (1). First, it is applied to the penetration of the short-range part of the PAR near the sea surface $dI/dz = k_2 I$, where $-1/k_2 << z < 0$, and second, it can be applied to the penetration of the long-range part of the PAR $dI/dz = k_1 I$, where $z << -1/k_1$ and where $k_2 >> k_1$ (see Tabs. 4 and 5). Details can be found in Appendix B.

For data fitting purposes, we applied MATLAB scripts that rely on the iterative Levenberg-Marquardt algorithm (Whittaker and Robinson, 1924) for nonlinear fitting. This method, however, requires the initial values for I and k in fitting the single-exponential function and I_1, I_2, k_1, and k_2 in fitting with the biexponential expression in (2). For this reason, we first applied a different equation to all reliable vertical profiles of PAR the semilog fit:

$$Y = \ln(I) = kz + \ln(I_0) \,, \tag{4}$$

which corresponds to the solution of (1). This widely used linearized fit serves as the ground for the single-exponential decrease in downward PAR irradiance. However, it also provides the initial value for the coefficients k and I_0 in the nonlinear single-exponential decrease of PAR with depth, as well as the initial value for the coefficient k_2 (and I_0) in the biexponential decrease of the PAR.

We rewrite the biexponential penetration of the PAR (2) in a more suitable form (Byun et al., 2014):

$$I(z) = I_0\left[Re^{k_1 z} + (1-R)e^{k_2 z}\right], \tag{5}$$

where R acts as the apportioning coefficient. In Byun et al. (2014), another coefficient–R' instead of R–is also introduced in the first term of the biexponential expression (5), indicating that just below the surface is $I(z) = I_0[R' + (1 - R)]$, which may easily differ from I_0, thus changing the meaning of I_0. Numerous fits with R' as the fourth fitting parameter provide results that were not a better match with the data than (5). Hence, we do not present results with the form applied by Byun et al. (2014).

It follows from (2) and (5) that $I_1 = I_0R$ and $I_2 = I_0(1–R)$. If $R = 0$, then $I(z) = I_0 \exp(k_2z)$ according to (5), so k_2 corresponds to k in (1), while if $R = 1$, $I(z) = I_0 \exp(k_1z)$. then k_1 corresponds to k. Therefore, we decided to initialize the coefficients in (5) in the following way: $R = 0$, $k_1 = 0$, $k_2 = k$. The change in the initial values, which indicate the robustness of the fitting method, is discussed in the results section.

Lee et al. (2005) studied the attenuation coefficient for visible downwelling solar radiation, denoted here as k, and for PAR light, they presented this with the following depth dependence:

$$k(z) = K_1 + \frac{K_2}{(1-z)^{0.5}}, \tag{6}$$

where the units of constants K_1 and K_2 are different, the one for K_2 is peculiar, and depth $z < 0$ is given in meters. By applying (6) to (1), which can be done by separating the variables and integrating, we obtain the solution

$$I(z) = I_0 e^{\left[K_1 z + 2K_2(1-\sqrt{1-z})\right]}, \tag{7}$$

into which we could fit our data as well. Although I_0 is initialized as in the other three cases, the only "reliable choice" of initialization of K_1 and K_2 was the one such that $K_1 = 0$ and $K_2 = k$, which is similar to the initialization with the biexponential expression.

In all nonlinear fitting methods (single-exponential form, biexponential form in (5), and (7), which follows from Lee et al. (2005)), the measured PAR values below the sea surface could be normalized by the PAR value $I(z_0)$ at the first depth. Therefore, nonlinear analytical fitting functions $I(z)$ are also divided by

I_0. In the semilogarithmic (linear) expression (4) of the (normalized) penetration to the depth of PAR, the Levenberg-Marquardt algorithm (Whittaker and Robinson, 1924), which is used for nonlinear fitting, is also applied, but in this iterative procedure, the coefficient $\ln(I_0)$ is fixed to zero (*i.e.*, $I_0 = 1$). This means that this fit also passes through the initial point (z_0, 1) in the profile of the PAR normalized data, just as other fitting functions do. The advantage of this normalization is twofold: parameter I_0 is eliminated from the set of fitting parameters, all of which are associated with the attenuation of PAR. Moreover, this concept is aligned with the normalized PAR profiles and the downward irradiance profiles for different water types, as described in Jerlov (1976), which are also applied here.

2.3. PAR and downward irradiance attenuation in water types

In numerical models of circulation, the downward irradiance is the input source of the energy within the water column, which is converted to heat. However, because vast "measurements of light" in a water column are conducted with much simpler measurements of PAR, we focus on the possible link between the vertical profiles of (downward) irradiance and PAR. However, the latter was introduced as the density flux of quanta (the number of photons per horizontal area per time) that is absorbed by plants (on land) for wavelengths between 400 nm and 700 nm by McCree (1971), who studied the quantum yield in this range of wavelengths.

The attenuation and spectrum of irradiance (350–2000 nm), as well as the downward irradiance and the density flux of quanta in the wavelength range 350–700 nm in seawater, is described thoroughly by Jerlov (1968, 1976), who also determines the attenuation of quanta with depth in this wavelength's range of light. On Jerlov (1976)'s Fig. 45 (page 116, see Eastern Mediterranean Sea), the spectral distribution of downward irradiance is represented for depths 0 m, 2 m, 5 m, 10 m, and 25 m for a "high solar elevation" (45°). The part of the spectral integral of downward irradiance between 350 nm and 400 nm (longer wavelengths part of UVA light) represents about 10–16% of the energy received in the water column in the wavelength's range of 350–700 nm. One can estimate this simply by using a trapezoidal integration of the spectral values at wavelengths separated for 50 nm. However, to obtain the share of the quanta of UVA, one divides each trapezoidal column by the central value of the wavelength. The share of quanta of UVA still does not surpass 16% of all quanta received by seawater of light with wavelengths 350–700 nm. It is unknown how this share of UVA differs in conditions when the PAR measurements were taken during the mornings around 9:02 h ± 0:53 h AM and under a solar elevation of 26.5° ± 10.9° (as described in the PAR measurements subsection). Although UV light has received much attention in the last few decades, especially in relation to ozone depletion (Bais et al., 2006), the share of UVA in the spectrum between 350 nm

and 700 nm has not been reanalyzed, and its dependence on solar elevation during the day has not been emphasized.

Therefore, keeping in mind that PAR measurements of quanta in the range 400–700 nm are smaller (for up to a few 10% at most), we can still estimate the attenuation coefficients for downward irradiance once we determine the water type from the PAR measurements. The part of the UVA light with longer wavelengths together with visible spectrum (350–700 nm) and of the total irradiance (350–2000 nm) for different water types has been classified by Jerlov (1976). Those plots of vertical profiles for different water types were digitized, and tables of values of vertical profiles were fitted with the biexponential expression, as will be presented in the results. At the sea surface, the PAR – or the irradiance – has a value of 100%. Therefore, the profiles were normalized according to the light intensity at the surface. Table 2 presents the digitized pairs of the PAR (percentage of downward surface PAR irradiance) and depths where the specific percentage was met for different water types, which is taken from Fig. 130 on page 197 of Jerlov (1976). For coastal waters, Fig. 132 in Jerlov (1976) presents the vertical profiles of the PAR as a percentage of the surface quanta. It is clear that the larger the type number, the smaller the depth of the PAR light penetration.

It is the attenuation of the total (downward) irradiance with a depth in coastal waters that matters in models of circulation of coastal waters, in which the irradiance (300–2500 nm) represents the heating source. This is a generator of stratification that induces vertical layering of circulation. For this reason, Tab. 28 on page 141 of Jerlov (1976), which contains the vertical profiles of irradiance in coastal waters, was utilized and is reproduced in Tab. 3.

Table 2. PAR in % of surface irradiance in 350–700 nm and depths for five coastal water types and one (III) oceanic type. The values are retrieved from Fig. 130 on page 197 of Jerlov (1976).

	Type III	Type 1	Type 3	Type 5	Type 7	Type 9
PAR [%]	Depth [m]	Depth [m]	Depth [m]	Depth [m]	Depth [m]	Depth [m]
100	0	0	0	0	0	0
70	1.69	1.32	0.95	0.73	0.57	0.33
50	3.43	2.84	2.00	1.41	1.01	0.68
40	4.71	3.89	2.75	1.87	1.32	0.92
20	9.24	7.66	5.24	3.52	2.42	1.74
10	14.30	12.00	8.00	5.26	3.65	2.68
5	19.65	16.85	11.07	7.13	4.97	3.61
4	21.21	18.33	12.03	7.70	5.37	3.92
2	26.52	23.40	15.29	9.61	6.75	4.95
1	31.85	28.73	18.48	11.57	8.00	6.00
0.5	37.70	34.19	21.69	13.51	9.46	7.11

Table 3. Irradiance (300–2500 nm) decrease with depth for for five coastal water types and one (III) oceanic type (from Jerlov (1976), Table 28 on page 141).

	Type III	Type 1	Type 3	Type 5	Type 7	Type 9
Depth [m]	I[%]	I[%]	I[%]	I[%]	I[%]	I[%]
0	100	100	100	100	100	100
1	39.4	36.9	33	27.8	22.6	17.6
2	30.3	27.1	22.5	16.4	11.3	7.5
5	16.8	14.2	9.3	4.6	2.1	1
10	7.6	5.9	2.7	0.69	0.17	0.052
20	0.97	1.3	0.29	0.02		
50	0.041	0.022				
75	0.0018					

3. Results

3.1. PAR on Vida and PAR on a vessel's probe in the air

We compared the PAR data measured on Vida (15 min average) versus the PAR data retrieved by casts of the MSS90 probe (7.7 s average time interval among all casts) from July 2011 to December 2015 (see Fig. 5). On any normal day, the maximum difference in time between the chosen PAR measured on Vida

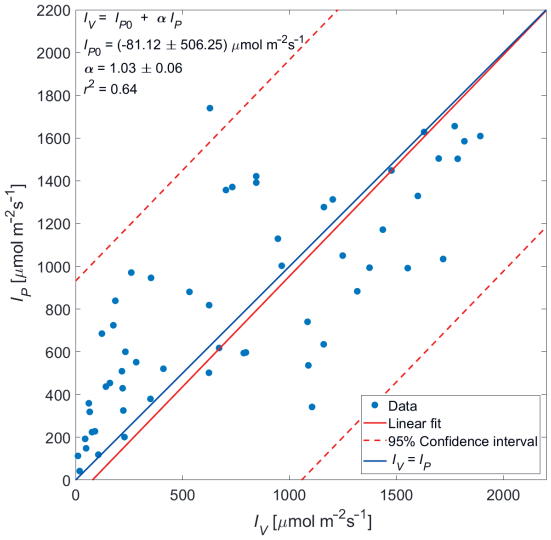

Figure 5. Surface values of the PAR I_P (average over the first 1.2 m values before the PAR sensor hits the water) versus the PAR measured at the buoy Vida I_V (4.5 m height). I_P is measured with the sensor on top of the probe between July 2011 and December 2015. The red line is the linear fit, the red dashed lines are the 95% confidence intervals, and the blue line is the line of exact agreement.

and PAR measured on the probe was 15 min. The scatter for the comparison of these different measurement methods around the ideal line was high ($r^2 = 0.64$). The majority of the PAR values on Vida were higher than the probe values. This is to be expected because the PAR sensor on the buoy was at a height of 4.5 m above the sea surface, while the PAR sensor on the probe was, at most, 1 m above it. The offset of higher PAR values on Vida is -81.12 ± 506.25 μmol m^{-2} s^{-1}, while the coefficient of proportionality is 1.03 ± 0.06.

3.2. PAR attenuation in the Gulf of Trieste (Northern Adriatic)

In studying the best estimate for describing the downward attenuation of PAR light, we begin with the fits on the mean vertical PAR profile obtained from 81 individual profiles (see Fig. 4, full red line). In Fig. 6, the plots of the four fitting methods are presented. Only the semilog fit is linear (black line), which is between the lines of the single-exponential decay of PAR (red line) and the biexponential decay (green line). Although the match of these two fits with the mean PAR data is good (Tab. 4, $r^2 = 0.94$), the fits with the biexpo-nential expression (5) and with the more complex attenuation—according to (7) (orange line), which follows from Lee et al. (2005)—are an excellent match (Tab. 4, $r^2 = 0.998$). The latter, however, shows a larger discrepancy (larger values) with the mean PAR profile data at depths of > 15 m.

We can notice from Tab. 4 that there are interesting values of attenuation coefficients. In the mono-exponential decrease, $k \leq 0.24$ m^{-1} and similar smaller values to this are attained by $k_1 = 0.13$ m^{-1} in the biexponential decrease, which is otherwise initialized with zero. The other coefficient of attenuation in the bi-exponential decrease of PAR $k_2 = 0.71$ m^{-1} is almost six times larger than k_1 and nearly four times larger than k. Obviously, the exponential decrease with the attenuation coefficient k_1 represents the long-range part of the penetration of

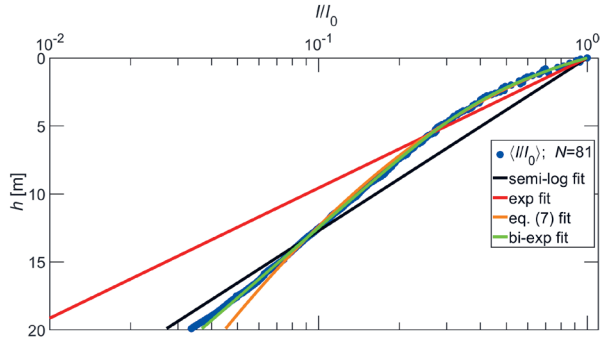

Figure 6. Representation of semilog (black line), exponential (red line), biexponential (green line), and Lee et al.'s (2005) method (Eq. (7), orange) of fitting over the mean PAR profile (dots), here composed of 81 PAR profiles. The profiles were normalized with the $I_0 = I(z_0)$, where z_0 is the first depth of the mean PAR value. Depth $h = -z$.

Table 4. Fitting coefficients of the fit over the mean profile of the PAR. Top table: single-exponential decrease of the PAR. Middle table: the biexponential decrease, bottom: PAR decrease according to (7), following Lee et al. (2005) Numbers next to the ± sign represent the 95% confidence intervals.

	k [m^{-1}]	r^2
$\ln(I/I_0) = kz$	0.18 ± 0.003	0.94
$I/I_0 = \exp(kz)$	0.24 ± 0.01	0.94

	k_1 [m^{-1}]	k_2 [m^{-1}]	R	r^2
$I/I_0 = R\exp(k_1 z) + (1-R)\exp(k_2 z)$	0.13 ± 0.01	0.71 ± 0.03	0.46 ± 0.02	0.998

	K_1 [m^{-1}]	K_2 [m$^{-1/2}$]	r^2
$I/I_0 = \exp(-K_1 z + 2K_2(1-\sqrt{1+z}))$	0.0014 ± 0.006	0.43 ± 0.01	0.998

the PAR, which is typical for the shorter (blue-green) wavelengths of light. The exponential decrease with the coefficient k_2 is the short-range part of penetration, which is typical for the longer wavelengths (orange-red) of the PAR. The apportioning coefficient R, which, according to (5), weighs the long-range part of the penetration, attains values of $R \cong 0.46$, meaning that the long-range part is smaller than the short-range part $(1-R)$ by around 10%. As seen from Tab. 4, the width of the 95% confidence intervals (which is twice the number next to the ± sign), ranges from less than 4% of the mean value (k in semilog fit) to an outstanding 857% for a very small value of K_1 (expression (7)), here with a median of 8%.

The sensitivity of the fitting method to the initialization values for biexponential expressions is quite robust. The fitting method is invariant to the initial values of apportioning the coefficients for R, and the fits are more sensitive to changes of the initial values of attenuation coefficients, which drive them in an exponential sense toward the solution. Still, the method is robust enough and converges to the same result by also applying an awkward initialization ($R = 0$ and $k_1 = k_2 = k$, or $k_1 = k_2 = 0$).

We ran all four fitting methods over all 81 "good" profiles of the PAR. It turns out that 12 of them had either an R or $(1-R) < 0$. Therefore, 69 profiles for which all coefficients are positive have been selected for statistics on the attenuation of the PAR light near the buoy Vida (Tab. 5). Because we have a sufficient number of "samples" (*i.e.*, profiles), out from which the statistics of the values of the coefficients could reliably be extracted, we can calculate the average value, the median value, and the SD for each coefficient. For five vertical profiles, the coefficient is $k_2 > 1$ (they are outliers: five values are between 134.8 m^{-1} and 6670.9 m^{-1}, with the median being 157.3 m^{-1}). Additional values are added in parentheses in Tab. 5 when these five profiles are also removed from the data set and when the statistical values differ. For these five profiles, the Secchi depth was found to be smaller (6.2 m ± 1.3 m) than usual (8.6 m ± 3.6 m), indicating that the waters

were more turbid than usual, even though the spread is large and turbidity via Secchi depth also affects k_1.

We notice from Tab. 5 that apart from k_2 (biexponential fit) and K_1 (according to (7)), the median value of attenuation coefficients and of the apportioning coefficient R is close to the average value. The ratio of the average and median value ranges between 101% and 122%, being the lowest for R ("no outliers"), and the largest for k is in the exponential fit and K_2 from (7). The largest discrepancy between the median and average value is for K_1 and k_2, when the average value is larger for two–and even three orders–of magnitude than the median value, indicating that the outliers heavily influence the average. The median values differ for these two parameters from an average value of about four (385% for k_2) to five times (517% for K_1) when five outliers are removed. The SD of the coefficients is between 36% (k in semilog fit and k_1 in biexponential fit) and 63% (K_2) of their average value when k_2 and K_1 are excluded. The SD of k_2 falls from 738% to 206% of their mean value when the k_2 outliers are excluded. The value of R suggests that 47% of the PAR is the long-range part. However, because of the relatively large value of SD, this part varies from 30% up to 64% of the PAR.

Table 5. The four fitting methods on 69 PAR vertical profiles. The notation "⟨⟩" means the average, "med" median value, and "SD" the standard deviation. At the bottom part of the table, the fit is presented with the expression that corresponds to (7), as suggested by Lee et al. (2005). Values in parenthesis are added for the statistics of the fitting quantities when additional vertical profiles of PAR are removed, for which $k_2 > 1$.

	$\ln(I/I_0) = kz$		$I/I_0 = \exp(kz)$	
	k [m^{-1}]	r^2	k [m^{-1}]	r^2
⟨⟩	0.19	0.87	0.27	0.78
med	0.17	0.92	0.23	0.88
SD	0.07	0.15	0.13	0.29

	$I/I_0 = R\exp(k_1 z) + (1–R)\exp(k_2 z)$			
	k_1 [m^{-1}]	k_2 [m^{-1}]	R	r^2
⟨⟩	0.14	3.20	0.48	0.96
med	0.12	0.83	0.48	0.98
SD	0.07	6.59	0.17	0.05

	$I/I_0 = \exp[K_1 z + 2K_2 (1 – (1–z)^{1/2})]$		
	K_1 [m^{-1}]	K_2 [m$^{-1/2}$]	r^2
⟨⟩	–0.02	0.50	0.93
med	0.003	0.41	0.97
SD	0.12	0.31	0.08

A word about goodness of fit (r^2) seems appropriate; this varies from 78% (mono-exponential fit) to 96% (biexponential fit) in the mean value. The discrepancy with the median value is the smallest for the biexponential fit (average versus median is 98%) and the largest for the mono-exponential fit (90 %). The SD is only 6% of the mean value in the (best) biexponential fit and reaches around 37% of the mean value in the mono-exponential fit.

We can now compare the values of the coefficients of attenuation of the mean PAR profile (Tab. 4) with the mean and median values extracted from the 69 profiles (Tab. 5). We can easily deduce that in both calculations, the mean and median values of the attenuation coefficient k in the semilog decrease of PAR $k = 0.17 - 0.19$ m^{-1} with SD = 0.07 m^{-1}. The mean and median values of the attenuation coefficient in the single-exponential decrease $k = 0.24 - 0.28$ m^{-1} with SD = 0.13 m^{-1}, while the median value is similar (0.23 m^{-1}). For the biexponential attenuation of the PAR, the mean value of the coefficient of the long-range attenuation nearly equals the value of the long-range attenuation of the mean profile; therefore, it stands that $k_1 = 0.14$ m^{-1}, with SD = 0.07 m^{-1} and the median being 0.13 m^{-1}. The coefficient of the short-range attenuation k_2 of the mean PAR profile (0.71 m^{-1}) is close to the median value of 69 profiles (0.85 m^{-1}) and is far below the average value (109 m^{-1}), or 3.2 m^{-1} (when outliers are excluded), with a huge SD (6.7 m^{-1} without outliers). For the depth-dependent expression (7) of the attenuation coefficients, in both calculations, K_1 is very close to zero, even slightly negative (–0.02 m^{-1}) when calculated from the 69 profiles (however, still much within the SD = 0.12 m^{-1}). The K_2 of the mean profile equals the median value of the 69 profiles (0.42 m$^{-1/2}$); however, the SD is quite large (0.32 m$^{-1/2}$). Nonetheless, we have now obtained a solid estimate of the attenuation coefficients of the PAR in shallow waters.

The values of r^2 in Tab. 5 suggest that from the perspective of fitting, both methods – the one with the biexponential expression and one with the depth-dependent attenuation coefficient (Lee et al., 2005) – are the best fit choices for the data used. By observing the values of K_1 (simple exponential dependence) that are practically "zero" with two orders of magnitude larger than the SD, one can deduce that for these data, the biexponential expression is still an adequate choice for the representation of the PAR data with the analytical expression.

3.3. PAR attenuation and Secchi depth

We also explore an inverse relationship between the attenuation coefficient of PAR k (in a single-exponential decay) and the depth Z_S at which the (white) Secchi disk (Secchi, 1864) vanishes, that is, $k_s = 1.4/Z_S$ (Stravisi, 1999). We have tested this relationship because the data of Z_S were provided in the same field campaigns as the PAR profiles were taken, and the results are presented in Fig. 7.

We consider the attenuation coefficient of PAR k in a semilog expression (subscript "L") and in a single-exponential decay (subscript "E"), along with k_1

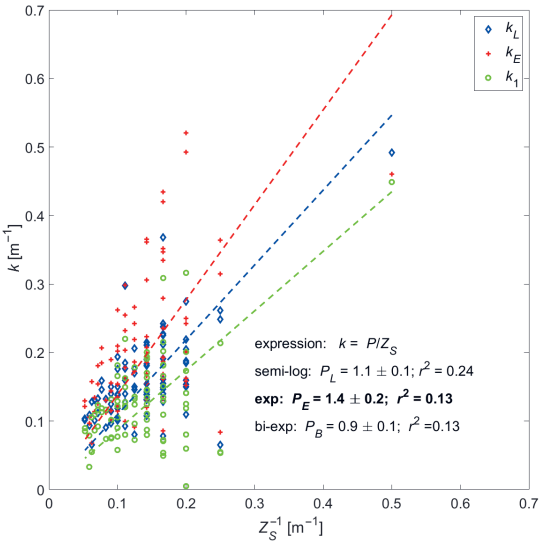

Figure 7. PAR attenuation coefficient k versus the inverse Secchi disk depth Z_S^{-1} The coefficient of proportionality P regarding the three methods of fitting, where the coefficient k is calculated from the fit with semilog expression (blue, subscript "*L*"), simple exponential expression (red, subscript "*E*"), and the biexponential expression ($k = k_1$, green, subscript "*B*"). Dashed colored lines represent the corresponding fits of the inverse relationships.

in the biexponential expression (5) (subscript "B"). The scatter is huge ($r^2 \leq 0.24$). However, among the poor fits, the best two are achieved, not surprisingly, with the coefficient of the semilog expression of PAR decay and of a single (nonlinear) exponential expression k_E, that is, $k_E = P_E/Z_S$, where for the latter $P_E = 1.4 \pm 0.2$.

3.4. PAR and downward irradiance attenuation in water types

The fitting results for PAR attenuation in the water types are presented in Tab. 2 and are summarized in Tab. 6.

Here, the more water types there are (more turbid water), the larger the values of k, k_1, and k_2 become because of stronger attenuation in coastal waters. The coefficient k follows this concept; however, there is a deviation from it in the more complicated attenuations of the PAR. The coefficient k_1 in biexponential expression falls from 0.33 m^{-1} in water type 5 to 0.24 m^{-1} in water type 7 (with the largest confidence interval of 0.74 m^{-1}), and it is much larger at its highest value 0.71 m^{-1} in water type 9. The value of coefficient k_2 is practically the same for water types 3 to 7, around 0.7 m^{-1}, while for water type 9, k_2 is larger by a factor of around 2.7. There are two other peculiarities with water type 7: the apportioning coefficient R is the largest for this water type (0.94), having the largest confidence interval (0.35 m^{-1}), while water type 9 has a similar value (0.35) as water type 3 (0.31). The second peculiarity of water type 7 concerns K_1,

Table 6. Fitting coefficients of the attenuation of quanta in the wavelength range 350–700 nm for Jerlov coastal water types (Jerlov, 1976). The values of r^2 are rounded to four decimals. Values next to a ± sign represent the 95% confidence intervals.

		Type III	Type 1	Type 3	Type 5	Type 7	Type 9
$\ln(I/I_0) = kz$	k[m^{-1}]	0.15±0.01	0.17±0.01	0.26±0.01	0.41±0.01	0.58±0.02	0.78±0.03
	r^2	0.991	0.982	0.989	0.995	0.995	0.991
$I/I_0 = \exp(kz)$	k[m^{-1}]	0.19±0.01	0.23±0.02	0.33±0.02	0.47±0.02	0.66±0.02	0.97±0.05
	r^2	0.996	0.995	0.997	0.999	0.999	0.998
$I/I_0 = R\exp(k_1z)$ $+(1–R)\exp(k_2z)$	R	0.4±0.04	0.39±0.08	0.31±0.085	0.53±0.29	0.94±0.35	0.35±0.08
	k_1[m^{-1}]	0.13±0.004	0.15±0.01	0.24±0.02	0.33±0.07	0.24±0.74	0.71±0.04
	k_2[m^{-1}]	0.37±0.02	0.49±0.08	0.74±0.15	0.67±0.15	0.71±0.16	1.88±0.26
	r^2	1	1	1	1	1	1
$I/I_0 = \exp[K_1z +$ $2K_2(1–(1–z)^{1/2})]$	K_1[m^{-1}]	0.1±0.01	0.09±0.006	0.15±0.006	0.31±0.04	0.54±0.18	0.30±0.37
	K_2[m$^{-1/2}$]	0.16±0.02	0.22±0.01	0.26±0.01	0.24±0.57	0.16±0.23	0.83±0.05
	r^2	1	1	1	1	1	1

which is the largest for this type (0.54 m^{-1}), displaying the largest confidence interval (0.74 m^{-1}), while water type 9 has a similar value as water type 5 (0.3 m^{-1}). K_2 behaves similarly to k_1: water type 7 "stands out" with its value of 0.17 m$^{-1/2}$ it is at maximum in water type 9 (0.83 m$^{-1/2}$). Although all expressions match the data very well (high r^2 values), the semilog expression looks to be the "poorest." The biexponential expression and the expression with the depth-dependent coefficient – (7) – match the data perfectly.

For these water types, the fitting coefficients for the biexponential fit of irradiance are summarized in Tab. 7. This expression matches the data excellently and has no redundant coefficients.

In the downward irradiance, k_1 and k_2 both increase with the number of water types (more turbid waters), as expected. This also holds for the apportioning coefficient R, indicating that more turbid waters have a slightly larger share of the long-range part of the irradiance, which can be attributed to shorter wavelengths of light.

Table 7. Fitting coefficients of irradiance I_I (300–2500 nm) penetration, normalized with the value below the sea surface $I_{I0,}$ for Jerlov coastal water types, r^2 is rounded to four decimals.

		Type III	Type 1	Type 3	Type 5	Type 7	Type 9
$I_I/I_{I0}=$ $R\exp(k_1z)+$ $(1–R)\exp(k_2z)$	R	0.58 ± 0.03	0.61 ± 0.04	0.61 ± 0.04	0.63 ± 0.02	0.66 ± 0.02	0.72 ± 0.01
	k_1[m^{-1}]	0.18 ± 0.02	0.2 ± 0.02	0.28 ± 0.03	0.42 ± 0.02	0.56 ± 0.02	0.66 ± 0.02
	k_2[m^{-1}]	2.69 ± 0.56	2.55 ± 0.52	2.83 ± 0.57	2.99 ± 0.22	3.04 ± 0.16	3.08 ± 0.09
	r^2	1	1	1	1	1	1

4. Summary and discussion

A comparison between the PAR measurements from the buoy Vida with Li-COR LI 190 SL 50 and from the underwater probe with Li-COR 192 in the air preceding vertical casts shows the linear proportionality as having a relatively large offset ($-81 \pm 506\ \mu mol\ m^{-2}\ s^{-1}$). The coefficient of proportionality 1.03 ± 0.06 is close to 1, even though it has a relatively high scatter ($r^2 = 0.64$). This can be attributed to several factors. The LI-COR instrument on a probe, as well as the one on a buoy, has a cosine correction, and as pointed out in the instruction manual (Anon., 2006a), this correction is overcompensated in the air, while an under compensation occurs in the water. Moreover, sailing cannot be done if weather conditions (sea state) reach a state of "3" according to the Beaufort scale (wavelet crests begin to break). Therefore, during the cruise, the waves with periods of 2–3 s at most are expected, and although the Li-COR 192 data on air were averaged over a mean time surpassing 6 s, some casts had a lower averaging time; perhaps, some wave motion was still affecting results and contributed to the scatter.

The comparison of the attenuation coefficient of PAR with the Secchi disk depth shows a large scatter ($r^2 \leq 0.24$) with the coefficient of the inverse relationship, $P_E = 1.4 \pm 0.2$, which matches the expression obtained by Stravisi (1999), where the confidence interval for the factor of proportionality is not written. However, in another work conducted on lake water (Bracchini et al., 2009), in which the PAR and upward irradiance relation were studied, the constant of the inverse proportionality between the attenuation coefficient of the PAR and Z_S is found to be 1.8 ± 0.02. Although the Secchi disk plate was always released on the shadow side of a vessel in the current study, there is no indication about whether the probe was released on the sunny side of a vessel, which could contribute to the scattering of the results. When the probe is lowered on a shadow side, the light may increase with depth at a certain point when the probe comes out from the underwater in the shadow of the vessel. Although clear cases of an increase of the PAR with depth were removed from the analysis, we have kept profiles that may be influenced by the vessel's shadow – the light near the sea surface could have been additionally damped. This may have contributed to the overall analysis of the PAR profiles, comparison of PAR measurements in the air with the ones on a buoy, and comparison of the PAR attenuation coefficient with the Secchi depth.

From Tabs. 4 and 5, we can see that the waters in the Gulf of Trieste, especially around the coastal buoy Vida, have for the attenuation coefficients of PAR k from 0.17 m^{-1} (semilog) to 0.28 m^{-1} (mono-exponential), and for the biexponential decrease, $k_1 = 0.13 - 0.14\ m^{-1}$ and $k_2 = 0.7 - 0.9\ m^{-1}$ (median values). The latter coefficient of the short-range part of PAR attenuation has the largest variability around the mean value (factor four of the mean value when outliers are removed). The apportioning coefficient R is around 0.47, indicating a nearly balanced share

between the longer-range and shorter-range parts of the PAR. However, from the values of coefficients of PAR attenuation, Tab. 6 shows that from the point of view of the attenuation coefficients k and k_1, the waters in the Gulf of Trieste (around the buoy Vida) fall in a type 3 ("turbid" oceanic water) and type 1 ("clear" *coastal* waters). From the point of view of k_2, they fall on the "other end" of coastal water types, that is, types 7 to 9. A reasonable explanation for this lies in the strong (density) stratification near the sea surface (Bogunović and Malačič, 2008; Malačič, 1991). Strong stratification near the surface maintains fine particles in a surface layer of the order of 1 m, thus increasing the turbidity of fresh water and increasing the attenuation of PAR. In this respect, we have additionally explored the seasonal variability of PAR attenuation and its variability with salinity. When the vertical profiles or PAR were grouped into four seasons, no clear seasonality in attenuation coefficient was apparent. One could deduce that the largest variability of PAR values is present in winter (not shown), when values range within four orders of magnitude below the sea surface ($10^{-1} - 10^{3}$ µmol m^{-2}s^{-1}), while near the bottom (to 20 m depth), they range within three orders of magnitude (10^{-1}–10^{2} µmol m^{-2} s^{-1}). Winter is followed by autumn in variability (10^{0}–10^{3} µmol m^{-2} s^{-1} near the sea surface and $10^{0} - 10^{2}$ µmol m^{-2} s^{-1} near the bottom). The last two are summer ($10^{1} - 10^{3}$ µmol m^{-2} s^{-1} near the surface, $10^{0} - 10^{2}$ µmol m^{-2} s^{-1} near the bottom) and spring ($10^{2} - 10^{3}$ µmol m^{-2} s^{-1} near the surface and $10^{1} - 10^{2}$ µmol m^{-2} s^{-1} near the bottom).

The variability of the attenuation coefficient k (mono-exponential fit) and Secchi depth on salinity S within the top 1 m is presented below (Fig. 8).

Although the scatter in k and Z_S with S is huge, as expected, one clearly notices that k decreases with S, especially for $S \leq 35$. With all the data (red

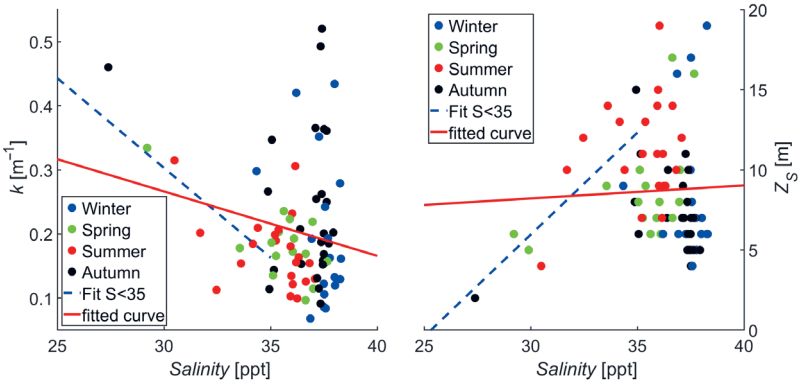

Figure 8. Attenuation the coefficient of k (*left*) and Secchi depth (*right*) as a function of salinity S, where the latter was averaged over the top 1 m of depth. The red line represents the linear fit over all the data, while the dashed blue line presents the fit only for the 13 data points for which $S \leq 35$ (fresher waters). The colors of the measurement dots represent seasons: winter (blue), spring (green), summer (red), and autumn (black).

curve), $\Delta k/\Delta S = -0.01\ \mathrm{m}^{-1} \pm 0.01\ \mathrm{m}^{-1}$. Yet if only data with $S \leq 35$ are consi-dered (dashed blue line): $\Delta k/\Delta S = -0.03\ \mathrm{m}^{-1} \pm 0.02\ \mathrm{m}^{-1}$). Z_S is increasing with S (all data: $\Delta Z_S/\Delta S = 0.1\ \mathrm{m} \pm 0.4\ \mathrm{m}$; if $S \leq 35$: $\Delta Z_S/\Delta S = 1.3\ \mathrm{m} \pm 0.7\ \mathrm{m}$). We also notice that in the summer and spring, PAR attenuation is generally lower and Z_S is higher.

Once the "classification" of waters is known from the attenuation of "extended PAR" (350–700 nm), we could presume that the same type of coastal waters are also prevalent from the point of view of irradiance. The range of shorter wavelengths of irradiance (300–450 nm) and of longer wavelengths (600–2500 nm) of irradiance are much broader than in the extended PAR irradiance. Nonetheless, water types 3 and 1, as shown in Tab. 7, indicate that downward irradiance is $k_1 = 0.2$–$0.28\ \mathrm{m}^{-1}$, while from types 7 and 9, a rough estimate $3.6 \pm 0.2\ \mathrm{m}^{-1}$ looks plausible for k_2. The apportion coefficient $R = 0.7 \pm 0.02$ seems a proper choice for downward irradiance.

In the setup of the NEMO model, Madec et al. (2019) applies the biexponential expression (in the subsection 4.4.2. Solar radiation penetration) of Paulson and Simpson (1977), which is denoted as the two-waveband formulation for the downward irradiance. However, it is pointed out that one band presents the IR band (wavelengths > 700 nm), which contributes to heating the upper few tens of centimeters. The attenuation coefficient for this band is $k_1 = 1/(0.35\ \mathrm{m}) = 2.86\ \mathrm{m}^{-1}$, and the apportioning coefficient is $R = 0.58$. However, in the waveband 400–700 nm, the ocean is more transparent with $k_2 = 1/(23\ \mathrm{m}) = 0.043\ \mathrm{m}^{-1}$, corresponding to (oligotrophic) water type 1 (Jerlow, 1968).

It should be noted that in our fits, the exponential term with k_1 (longer-range attenuation) is multiplied by R, while in Madec et al. (2019) and in Paulson and Simpson (1977) the shorter-range exponential term with k_2 (shorter range) is multiplied by R. Therefore, k_1 in our work should be compared with k_2 in previous findings and vice versa, and $(1–R)$ in our work should be compared with R in previously mentioned publications. Our suggestion for $(1–R) = 0.3 \pm 0.02$ does not compare well with the value 0.58 of Madec et al. (2019). Here, the discrepancy is larger in the long-range attenuation of downward irradiance (not PAR) 0.2–$0.28\ \mathrm{m}^{-1}$ (coastal turbid waters) with $0.043\ \mathrm{m}^{-1}$ (Madec et al., 2019), indicating between a five and six times larger "long" range *attenuation* in ocean waters (of the northern Adriatic Sea). The short-range attenuation of irradiance $3.6\ \mathrm{m}^{-1} \pm 0.2\ \mathrm{m}^{-1}$ also surpasses the value $2.86\ \mathrm{m}^{-1}$ described in the NEMO manual (Madec et al., 2019), here by a factor of 1.26. Therefore, in numerical models for coastal waters (the Gulf of Trieste), R will be roughly doubled, the long-range coefficient of attenuation will be multiplied by a factor of five to six, and the short-range coefficient of attenuation multiplied by 1.2 to 1.3. Final say about these changes will result from the validation of numerical simulations of circulation and heating of coastal waters with observations that need to take place in the future.

Madec et al. (2019) also refers to Morel (1988), who points out that the biexponential decrease of irradiance has been shown to provide a very crude and

simplistic representation of the observed light penetration profiles because light absorption in the ocean is spectrally selective and depends on particle concentration. Morel (1988) offers an accurate representation of light penetration using a 61-waveband formulation, which is computationally extensive and requires data. A simplified version with the attenuation of light in three wavebands blue (400–500 nm), green (500–600 nm), and red (600–700 nm) is offered by Lengaigne et al. (2007), in which for each waveband, the chlorophyll-dependent attenuation coefficient is fitted to the coefficients computed from the full spectral model of Morel and Maritorena (2001). This concept, of course, requires surface satellite chl-*a* content, if not also the chl-*a* vertical profiles.

The studies of Lee et al. (2005) and Lee et al. (2018), which support the depth dependence of attenuation coefficients (6), are also very useful in clarifying the dependence of the "bulk" properties (*e.g.*, the attenuation coefficient) of light with the IOPs that are spectral quantities. However, this requires in-depth knowledge of marine optics, which is usually lacking in institutions that study marine ecology.

The PAR measurements conducted over the last few decades comprise a narrowed spectral band of quanta than that described by Jerlov (1976) and that the PAR quanta tends to be lower by 10–16%, which implies the increase of the deviation of k_1, k_2, and R from the estimated values.

We have demonstrated that the mono-exponential expression and the semilog expression yield a relatively modest match with the PAR profile data. However, initializing the coefficients in the nonlinear least-square fits with coefficients from them is a solid choice (especially when using the semilog one). The biexponential expression with one apportion coefficient seems the most reasonable choice that offers the sound logic of separating the PAR irradiance into two parts, one with a slightly dominating long range (shorter wavelengths) and one with a slightly less expressed short range (longer wavelengths). Needless to say, in coastal seas, the variability of light penetration is large, and simulating the circulation of water masses under specific (synoptic) conditions requires some additional information about the light in the water column, which is to be obtained either by in-situ measurements or by remote sensing methods.

We have also clearly demonstrated that the biexponential representation of the PAR in coastal waters of the Northern Adriatic Sea is at least as good as the one that follows from the depth dependence of the attenuation coefficient of the PAR (Lee et al., 2005).

When there is no possibility of PAR measurements through the water column, the "simple" Secchi method may represent a "way out" for marine ecologists regarding PAR light attenuation. Although the scatter is large, a reasonable expression, first laid out by Stravisi (1999), is confirmed: $k = P_E/Z_S$, where $P_E = 1.4 \pm 0.2$. The proportionality factor P_E is well within the limits of values in

Table 1 of Lee et al. (2018), where an extensive analysis on the relationship between the Secchi disk depth and attenuation coefficient can be found.

Acknowledgements – The authors acknowledge the financial support of the Slovenian Research Agency (research core funding No. P1-0237) and program for young researchers in accordance with the agreement on (co)financing research activities in 2018.

References

Anonymus (2005): *LI-COR terrestrial radiation sensors, instruction manual*. Li-COR, Inc., Lincoln, NE, 31 p.

Anonymus (2006a): *LI-COR underwater radiation sensors, instruction manual*. Li-COR, Inc., Lincoln, NE, 31 p.

Anonymus (2006b): *Microstructure profiler MSS90, operating instructions user's manual*, ver 5 ed. Sea&Sun Technology, Trappenkamp, Germany, 57 p.

Anonymus (2007): *MSSpro microstructure data evaluation tool, User manual*. ISW Wassermesstechnik Dr. Hartmut Prandke, Fünfseen OT Petersdorf, Germany, 45 p.

Bais, A., Lubin, D., Arola, A., Bern, G., Blumthaler, M., Chubarova, N., Haspel, C., Gies, H. P., Krotkov, N., Lantz, K., Mayer, B., McKenzie, R., Piacentini, R., Seckmeyer, G., Slusser, J. R. and Zerefos, C. (2006): Surface ultraviolet radiation: Past, present and future (Chapter 5). *Scientific assessment of ozone depletion: 2006; Global Ozone Research and Monitoring Project*, World Meteorological Organization, 58 p, available at https://www.researchgate.net/publication/227860247_Surface_ultraviolet_radiation_Past_present_and_future

Bogunović, B. and Malačič, V. (2008): Circulation in the Gulf of Trieste: Measurements and model results, *Nuovo Cimento C*, **31**, 301–326, https://doi.org/10.1393/ncc/i2008-10310-9.

Bracchini, L., Dattilo, A. M., Hull, V., Loiselle, S. A., Tognazzi, A. and Rossi, C. (2009): Modelling upwelling irradiance using Secchi disk depth in lake ecosystems, *J. Limnol.,* **68**, 83–91, https://doi.org/10.4081/jlimnol.2009.83.

Byun, D.-S., Wang, X. H., Hart, D. and Zavatarelli, M. (2014): Review of PAR parameterizations in ocean ecosystem models, *Estuar. Coast. Shelf S.,* **151**, 318–323, https://doi.org/10.1016/j.ecss.2014.05.006.

Duntley, S. and Preisendorfer, R. (1952): *The visibility of submerged objects*. Final Report to Office of Naval Research, 36 p, available at https://escholarship.org/content/qt2mz4d121/qt2mz4d121.pdf?t=lnr31h.

GmbH, S. S. T. (2021): *Microstructure probe MSS 90*.

Hedström, K. S. (2009): *Draft technical manual for a coupled sea-ice/ocean circulation model (version 3)*. US Department of the Interior Minerals Management Service Anchorage, Alaska (Contract No. M07PC13368).

Jerlov, N. G. (1968): *Optical oceanography*. Elsevier, Amsterdam, 194 p, https://doi.org/10.4319/lo.1968.13.4.0731.

Jerlov, N. G. (1976): *Marine optics*. Elsevier, Amsterdam, 230 p.

Kirk, J. T. O. (1994): *Light and photosynthesis in aquatic ecosystems. 2nd Edition*. Cambridge University Press, Cambridge, https://doi.org/10.1017/CBO9780511623370.

Lee, Z., Du, K., Arnone, R., Liew, S. and Penta, B. (2005): Penetration of solar radiation in the upper ocean: A numerical model for oceanic and coastal waters, *J. Geophys. Res. – Oceans*, **110**, C09019, https://doi.org/10.1029/2004JC002780.

Lee, Z., Shang, S., Du, K. and Wei, J. (2018): Resolving the long-standing puzzles about the observed Secchi depth relationships, *Limnol. Oceanogr.*, **63**, 2321–2336, https://doi.org/10.1002/lno.10940.

Lengaigne, M., Menkes, C., Aumont, O., Gorgues, T., Bopp, L., André, J.-M. and Madec, G. (2007): Influence of the oceanic biology on the tropical Pacific climate in a coupled general circulation model, *Clim. Dyn.*, **28**, 503–516, https://doi.org/10.1007/s00382-006-0200-2.

Madec, G., Bourdallé-Badie, R., Chanut, J., Clementi, E., Coward, A., Éthé, C., Iovino, D., Lea, D., Lévy, C., Lovato, T., Martin, N., Masson, S., Mocavero, S., Rousset, C., Storkey, D., Vancoppenolle, M., Müller, S., Nurser, G., Bell, M. and Samson, G. (2019): *NEMO ocean engine, scientific notes of climate modelling center*. Institut Pierre-Simon Laplace (IPSL), Paris, 273 p.

Malačič, V. (1991): Estimation of the vertical eddy diffusion coefficient of heat in the Gulf of Trieste (Northern Adriatic), *Oceanol. Acta,* **14**, 23–32.

McCree, K. J. (1971): The action spectrum, absorptance and quantum yield of photosynthesis in crop plants, *Agr. Meteorol.*, **9**, 191–216, https://doi.org/10.1016/0002-1571(71)90022-7.

Meier, H. M. (2001): On the parameterization of mixing in three-dimensional Baltic Sea models, *J. Geophys. Res. – Oceans*, **106**, 30997–31016, https://doi.org/10.1029/2000JC000631.

Mellor, G. L. (2004): *Users guide for a three-dimensional, primitive equation, numerical ocean model (June 2003 version)*. Program in Atmospheric and Oceanic Sciences, Princeton University, Princeton, 53 p., available at https://www.researchgate.net/publication/242777179_Users_Guide_For_A_Three-Dimensional_Primitive_Equation_Numerical_Ocean_Model

Morel, A. (1988): Optical modeling of the upper ocean in relation to its biogenous matter content (case I waters), *J. Geophys. Res. – Oceans*, **93,** 10749–10768, https://doi.org/10.1029/JC093iC09p10749.

Morel, A. and Maritorena, S. (2001): Bio-optical properties of oceanic waters: A reappraisal, *J. Geophys. Res. – Oceans*, **106**, 7163–7180, https://doi.org/10.1029/2000JC000319.

Paulson, C. A. and Simpson, J. (1977): Irradiance measurements in the upper ocean, *J. Phys. Oceanogr.*, **7**, 952–956, https://doi.org/10.1175/1520-0485(1977)007<0952:IMITUO>2.0.CO;2.

Secchi, P. A. (1864): Relazione delle esperienze fatte a bordo della pontificia pirocorvetta Imacolata Concezione per determinare la trasparenza del mare, in: *Memoria del P. A. Secchi. Il Nuovo Cimento Giornale de Fisica, Chimica e Storia Naturale, Ottobre 1864*, Published 1865, **20**, 205–237 (in Italian).

Stravisi, F. (1999): Optical seawater properties in the Gulf of Trieste, *Boll. Soc. Adr. Sci.,* **79**, 61–75.

Talley, L. D. (2011): An introduction, in: *Descriptive physical oceanography: 6th edition*, edited by: Talley, L. D., Pickard, G. L., Emery, W. J. and Swift, J. H. Academic Press, Boston.

Talley, L. D., Pickard, G. L., Emery, W. J. and Swift, J. H. (2011): Physical properties of seawater, in: *Descriptive physical oceanography, 6th Edition*, edited by: Talley, L. D., Pickard, G. L., Emery, W. J. and Swift, J. H. Academic Press, Boston, 29–65.

Whittaker, E. T. and Robinson, G. (1924): *The calculus of observations: An introduction to numerical analysis*. Dover Publication, 394 pp.

SAŽETAK

Bieksponencijalno slabljenje fotosintetički aktivnog zračenja (PAR) u obalnim vodama (Sjeverni Jadran)

Borut Umer i Vlado Malačič

Koeficijenti slabljenja fotosintetski aktivnog zračenja (PAR) određeni su iz vertikalnih profila PAR-a u obalnim vodama (Tršćanski zaljev, Sjeverni Jadran). Okomiti profili sakupljani su približno dva puta mjesečno od srpnja 2011. do prosinca 2015. godine, a vrijednosti PAR-a neposredno iznad morske površine uspoređivane su s podacima PAR-a izmjerenim na plutači.

Ovo istraživanje podupire nelinearnu ovisnost PAR-a o dubini primjenom biekspo-nencijalnog izraza, što daje puno bolju podudarnost s podacima nego primjenom monoeksponencijalnog izraza. Osim toga, biekseponencijalno slabljenje PAR-a s dubinom je rješenje homogene diferencijalne jednadžbe drugog reda. Temeljem analize koeficijenata prigušenja PAR-a predložena je metoda za procjenu tipa vode. Utvrđeno je da za odabranu lokaciju (Tršćanski zaljev) koeficijent slabljenja kod primjene monoeksponencijalne relacije PAR-a iznosi 0,19–0,21 m^{-1}, dok kod primjene biekseponencijalne relacije koeficijent slabljenja PAR-a iznosi 0,12–0,14 m^{-1} (zračenje dugog dosega), odnosno 0,8–0,9 m^{-1} (zračenje kratkog dosega). Prethodno navedeni rezultati vode do zaključka da se veći dio vodenog stupa podudara s obalnim vodama tipa 1, dok je površinski sloj sastavljen od obalnih voda tipa 7 ili 9. Koeficijenti slabljenja dolaznog zračenja, iz procjene zastupljenih tipova voda, iznose 0,19 $m^{-1} \pm 0{,}01$ m^{-1} (zračenje dugog dosega) i 3,0 $m^{-1} \pm 0{,}7$ m^{-1} (zračenje kratkog dosega). Pomoću ovih koeficijenata može se odrediti izvor topline unutar vodenog stupca.

Ključne riječi: PAR, koeficijent slabljenja, zračenje, dubina Secchi diska, metode fitanja

Corresponding author's address: Borut Umer, National Institute of Biology, Marine Biology Station Piran, Fornače 41, SI-6330 Piran, Slovenia; tel: +386 (0)59 232 944; e-mail: borut.umer@nib.si

Appendix A

Here, the bi-exponential expression is the solution of (3). When the exponential solution exp(kz) is inserted in (3), the equation for the roots of the attenuation coefficient k follows the quadratic equation:

$$Ak^2 + Bk + C = 0\,, \tag{A1}$$

which leads to the biexponential solution (2) only if $B^2 - 4AC > 0$. Moreover, we require that both solutions for the attenuation coefficient

$$k_{1,2} = \frac{-B \pm \sqrt{B^2 - 4AC}}{2A} \tag{A2}$$

be positive so that I can decrease with depth ($-z > 0$) with both coefficients k_1 and k_2. This requires that $B < 0$ and also that $0 < \sqrt{B^2 - 4AC} < -B$ or that $C > 0$.

We may rewrite eq. (A1) in the form of two first-order equations:

$$\frac{dI}{dz} = Y; \quad \frac{dY}{dz} = -bY - cI\,, \tag{A3}$$

where $b = B/A$ and $c = C/A$. The variability $I(z)$ differs from (1) in that dI/dz is no longer proportional to $I(z)$ but is some function of depth $Y(z)$, where the rate of variability of the latter, dY/dz, is proportional to a linear combination of Y itself and also of I. One may also easily retrieve from (A2) the coefficients b and c from the attenuation coefficients k_1 and k_2 once they are determined from the least-square fit of the profile $I(z)$ with the biexponential function because $b = -(k_1 + k_2)$ and $c = k_1k_2$. If, however, $c = 0$, then one obtains

$$\frac{d^2I}{dz^2} = -b\frac{dI}{dz}, \tag{A6}$$

which is similar to (1), apart for the integration constants. For the latter, if one also supposes that at the surface $\frac{dI}{dz}(z = 0) = -kI_0$, when integrating from the surface $z = 0$, then (1) follows from (7), and the single-exponential decrease of downward irradiance is retrieved.

Appendix B

According to the findings in Appendix A, (3) can be rewritten as follows:

$$I'' - (k_1 + k_2)I' + k_1k_2I = 0\,, \tag{B1}$$

where prime denotes the derivative with respect to z. Assume that $k_2 >> k_1$ and note that the solution is in biexponential form (5), which means that $I = I_L + I_S$, where the long-range part of PAR $I_L = I_{L0}\, exp(k_1 z)$ and the short-range part $I_S = I_{S0}\, exp(k_2 z)$ and where their values at the sea surface are $I_{L0} = I_0\, R$ and $I_{S0} = I_0\, (1- R)$, respectively. Near the sea surface, where $-1/k_2 << z < 0$, the exponential decay e^{-1} of the short-range part of PAR I_S is linearized and proportional to $1+ k_2 z$. This linearization near the sea surface holds even better for the long-range part of PAR I_L, which is proportional to $1+ k_1 z$ and varies much less within this surface layer than I_S. Thus, the second derivative of I_L with z is very weak compared with the second derivative of I_S:

$$I_L'' \propto k_1^2(1 + k_1 z) \ll k_2^2(1 + k_2 z) \propto I_S'' \,. \tag{B2}$$

Therefore, the second derivative I'' in (B1) is dominated by I_S''. For this near-surface layer, it also follows that for I_S, the second term in (B1) (first derivative) is much larger than the third term:

$$(k_1 + k_2)k_2(1 + k_2 z) \gg k_1 k_2(1 + k_2 z) \,, \tag{B3}$$

where it can be easily shown that the first and second terms in (B1) for I_S are of the same order.

On the other hand, the short-range I_S is practically absent at larger depths, for $z << -1/k_1$. Therefore, in this depth range, the third term in (B1) I is predominantly determined by I_L. Moreover, for I_L, in this range of z the first term in (B1) (second derivative) is much smaller than the second (first derivative):

$$k_1^2 \exp(k_1 z) \ll (k_1 + k_2) \exp(k_1 z) \,. \tag{B4}$$

Because (B1) is linear and homogeneous, it can be decomposed into the equation for only I_S and the same equation for I_L. Considering the above approximations, (B1) for $-1/k_2 << z < 0$ for the short-range part of PAR gives the following equation for I_S:

$$I_S'' - (k_1 + k_2) I_S' \cong 0 \,, \tag{B5}$$

which, after integration of $z >> -1/k_2$ to 0, becomes

$$I_S' \cong (k_1 + k_2) I_S \cong k_2 I_S \,, \tag{B6}$$

where we have taken into account that (B6) also holds for $z = 0$. It also seems appropriate to point out that in this near-surface layer $I \cong I_0\, (1–R)(1 + k_2)z = I_S$ because $k_2 >> k_1$ and when R is not very close to 1 (see Tables 4, 5, and 7). Therefore, (B6) is also valid for I, which is the "total" downward penetration of the PAR in the near-surface layer.

However, for $z << -1/k_1$, the long-range part of the PAR is well described by

$$(k_1 + k_2)I_L' \cong k_1 k_2 I_L \,,$$

which, because of $k_2 >> k_1$, becomes

$$I_L' \cong k_2 I_L \,. \tag{B7}$$

At these depths, $I \cong I_L$ because I_S is already extinguished at depths between $-1/k_2$ and for $-1/k_1$. Thus, we conclude that the second-order differential equation (3) or (B1) satisfies Beer's first-order law of light attenuation near the sea surface and at greater depths. Whether one would derive (3) from (B5) and (B7) is another matter.